



Volume II

Appendix D.5

Space Weather Conditions

This appendix provides a detailed discussion of space weather (the action of highly energetic particles, primarily from the Sun, in the outer layer of the Earth's atmosphere) and the potential effects of space weather on the Orbiter on February 1, 2003. This investigation was originally prompted by public claims of unusually active space weather conditions during the mission and by a photograph that claimed to show a lightning bolt striking *Columbia* at an altitude of 230,000 feet over California during re-entry. The report concludes that space weather was unlikely to have played a role in the loss of *Columbia*.

This is a document commissioned by the Columbia Accident Investigation Board and is published here as written, without editing. The conclusions drawn in this report do not necessarily reflect the conclusions of the Board; when there is a conflict, the statements in Volume I of the Columbia Accident Investigation Board Report take precedence.

THIS PAGE INTENTIONALLY LEFT BLANK



Space Weather Conditions

Submitted by William J. Burke, Space Vehicle Directorate, Air Force Research Laboratory
Joseph M. Kunches, National Oceanic and Atmospheric Administration Space Environment Center

Space Weather Conditions on February 1, 2003



William J. Burke
Space Vehicles Directorate
Air Force Research Laboratory



Joseph M. Kunches
National Oceanic and Atmospheric Administration
Space Environment Center

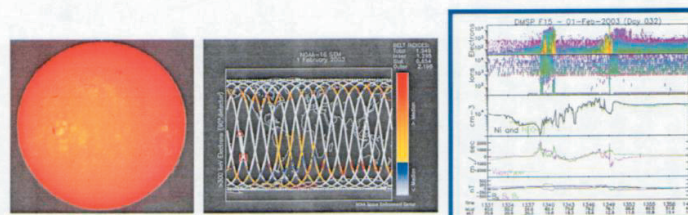


Table of Contents

1.0	Introduction	3
2.0	A Space Weather Tutorial	3
2.1	Working Definitions	3
2.2	Space Weather Characteristics	4
2.3	Solar Effects	5
2.4	Radiation Effects	9
2.5	Equatorial Plasma Bubbles	11
3.0	Space Weather Conditions on February 1, 2003	12
3.1	Interplanetary Measurements from ACE	12
3.2	LEO Measurements from DMSP	13
3.3	LEO Measurements from POES	18
3.4	Charging Effects	20
3.5	Geostationary Orbit Measurements	21
3.6	Ground Based Measurements	25
4.0	Summary and Conclusions	27
5.0	Acronyms	28

2

BO-000027 addition -
SFOML-WING-6-14.pdf

CTF091-1758

Geospace Weather Conditions on February 1, 2003

William J. Burke
Air Force Research Laboratory
Space Vehicles Directorate
Hanscom AFB, MA 01731

Joseph M. Kunches
National Oceanic and Atmospheric Administration
Space Environment Center
Boulder, CO 80305

1.0 Introduction

This report considers the possibility that space weather conditions played a role in the loss of the space shuttle Columbia. It was first presented to the Columbia Accident Investigation Board (CAIB) in Houston, Texas, on March 3, 2003, consequent to reported observations that a coronal mass ejection (CME) driven shock passed the Earth on February 1, 2003. The first part of this report is a tutorial on space weather with emphasis on the electrodynamics of the geospace environment. The second part reviews plasma, particle, and field measurements taken on February 1, 2003, from multiple space and ground based sources. These data clearly show that up to the time of the loss of Columbia, at approximately 14:09 Greenwich Mean Time (GMT), the geospace environment was quiet. Effects of the CME were not observed at Earth until several hours after the accident. It is highly unlikely that any known space weather effect played a role in the loss of Columbia.

2.0 A Space Weather Tutorial

We begin the tutorial with several working definitions, then examine specific space weather characteristics for both typical and stormtime conditions.

2.1 Working Definitions

The term "space weather" describes the systematic variability of geospace environments that occurs on day-to-day or shorter time scales and affects the performance of space related systems. We distinguish weather from climatological effects that occur on year-to-year or solar-cycle time scales. "Systematic variability" refers to repeatedly observed phenomena whose main lines of causality are understood. The "geospace environment" includes the region around the Earth extending from an altitude of approximately 60 km to the magnetopause. The magnetopause is the boundary between regions dominated by the Earth's magnetic field and interplanetary

3

BO-000027 addition -
SFOML-WING-6-14.pdf

CTF091-1759

plasmas, particles, and fields. The Sun is the ultimate source of most space weather effects. Meteorites, galactic cosmic rays, and tropospheric electric fields are notable exceptions. However, the internal or coupled electrodynamics of the magnetosphere and ionosphere generally represent the immediate causes of space weather effects. The systems affected by space environmental changes are many, ranging from orbiting satellites to communications links and electrical power distribution networks.

Before considering actual space weather measurements it is useful to recognize that space physicists think in terms of a multi-dimensional world. In addition to the normal three dimensions of our every day lives, they also consider the energies or ionization states as added dimensions characterizing particle environments found in geospace. For example, the "plasmasphere" and the "radiation belts" occupy almost the same region of physical space. However, plasmaspheric particles have thermal energies of a few electron volts (eV) while radiation belt particle energies are in the millions of electron volts (MeV) range. The terms "thermosphere" and "ionosphere" describe different particles of the same energies, neutral and ionized atoms and molecules, respectively, which are found in the same region of space at altitudes above 60 km. Most names given to describe the different regions of space are phenomenological and were assigned by their discoverers. The term "radiation belts" probably reflects the shocked reaction of one of Professor James Van Allen's graduate students to the first Geiger counter measurements on Explorer 1, "Space is radioactive!"

2.2 Space Weather Characteristics

In considering space weather effects it is useful to have some idea of the differences between typical and disturbed conditions (Table 1). The driver for most geospace weather lies in the solar wind that originates in the Sun's corona and terminates at the boundary with interstellar space. At 1 astronomical unit (AU), the distance between the Sun and Earth (~1.5 10^8 km), typical solar wind densities and speeds are approximately 5 cm^{-3} and 400 km/s, respectively. Under disturbed conditions they can rise to greater than 20 cm^{-3} and 1,000 km/s, respectively. The dynamic pressure of the solar wind (~1 nano-Pascal (nPa)) compresses the Earth's magnetic field on the dayside and extends it into a long cylinder called the magnetotail. The convenient unit for measuring distance in the magnetosphere is an Earth radius ($1 R_E = 6387 \text{ km}$). Under typical conditions the subsolar magnetopause is at ~10 R_E . When conditions become disturbed the solar wind's dynamic pressure can exceed 10 nPa and the magnetopause is pushed earthward of geostationary orbit (~6.6 R_E).

Table 1. Solar Wind Characteristics		
Parameter	Typical	Disturbed
Density	$5 - 10 \text{ cm}^{-3}$	$20 - 100 \text{ cm}^{-3}$
Velocity	400 km/s	700 km/s
Pressure	$1 - 2 \text{ nPa}$	$> 10 \text{ nPa}$
IMF	$5 - 10 \text{ nT}$	$20 - 60 \text{ nT}$

4

BO-000027 addition -
SFOML-WING-6-14.pdf

CTF091-1760

plasmas, particles, and fields. The Sun is the ultimate source of most space weather effects. Meteorites, galactic cosmic rays, and tropospheric electric fields are notable exceptions. However, the internal or coupled electrodynamics of the magnetosphere and ionosphere generally represent the immediate causes of space weather effects. The systems affected by space environmental changes are many, ranging from orbiting satellites to communications links and electrical power distribution networks.

Before considering actual space weather measurements it is useful to recognize that space physicists think in terms of a multi-dimensional world. In addition to the normal three dimensions of our every day lives, they also consider the energies or ionization states as added dimensions characterizing particle environments found in geospace. For example, the "plasmasphere" and the "radiation belts" occupy almost the same region of physical space. However, plasmaspheric particles have thermal energies of a few electron volts (eV) while radiation belt particle energies are in the millions of electron volts (MeV) range. The terms "thermosphere" and "ionosphere" describe different particles of the same energies, neutral and ionized atoms and molecules, respectively, which are found in the same region of space at altitudes above 60 km. Most names given to describe the different regions of space are phenomenological and were assigned by their discoverers. The term "radiation belts" probably reflects the shocked reaction of one of Professor James Van Allen's graduate students to the first Geiger counter measurements on Explorer 1, "Space is radioactive!"

2.2 Space Weather Characteristics

In considering space weather effects it is useful to have some idea of the differences between typical and disturbed conditions (Table 1). The driver for most geospace weather lies in the solar wind that originates in the Sun's corona and terminates at the boundary with interstellar space. At 1 astronomical unit (AU), the distance between the Sun and Earth (~1.5 10^8 km), typical solar wind densities and speeds are approximately 5 cm^{-3} and 400 km/s, respectively. Under disturbed conditions they can rise to greater than 20 cm^{-3} and 1,000 km/s, respectively. The dynamic pressure of the solar wind (~1 nano-Pascal (nPa)) compresses the Earth's magnetic field on the dayside and extends it into a long cylinder called the magnetotail. The convenient unit for measuring distance in the magnetosphere is an Earth radius ($1 R_E = 6387 \text{ km}$). Under typical conditions the subsolar magnetopause is at ~10 R_E . When conditions become disturbed the solar wind's dynamic pressure can exceed 10 nPa and the magnetopause is pushed earthward of geostationary orbit (~6.6 R_E).

Table 1. Solar Wind Characteristics		
Parameter	Typical	Disturbed
Density	$5 - 10 \text{ cm}^{-3}$	$20 - 100 \text{ cm}^{-3}$
Velocity	400 km/s	700 km/s
Pressure	$1 - 2 \text{ nPa}$	$> 10 \text{ nPa}$
IMF	$5 - 10 \text{ nT}$	$20 - 60 \text{ nT}$

4

BO-000027 addition -
SFOML-WING-6-14.pdf

CTF091-1760

plasmas, particles, and fields. The Sun is the ultimate source of most space weather effects. Meteorites, galactic cosmic rays, and tropospheric electric fields are notable exceptions. However, the internal or coupled electrodynamics of the magnetosphere and ionosphere generally represent the immediate causes of space weather effects. The systems affected by space environmental changes are many, ranging from orbiting satellites to communications links and electrical power distribution networks.

Before considering actual space weather measurements it is useful to recognize that space physicists think in terms of a multi-dimensional world. In addition to the normal three dimensions of our every day lives, they also consider the energies or ionization states as added dimensions characterizing particle environments found in geospace. For example, the "plasma sphere" and the "radiation belts" occupy almost the same region of physical space. However, plasmaspheric particles have thermal energies of a few electron volts (eV) while radiation belt particle energies are in the millions of electron volts (MeV) range. The terms "thermosphere" and "ionosphere" describe different particles of the same energies, neutral and ionized atoms and molecules, respectively, which are found in the same region of space at altitudes above 60 km. Most names given to describe the different regions of space are phenomenological and were assigned by their discoverers. The term "radiation belts" probably reflects the shocked reaction of one of Professor James Van Allen's graduate students to the first Geiger counter measurements on Explorer 1, "Space is radioactive!"

2.2 Space Weather Characteristics

In considering space weather effects it is useful to have some idea of the differences between typical and disturbed conditions (Table 1). The driver for most geospace weather lies in the solar wind that originates in the Sun's corona and terminates at the boundary with interstellar space. At 1 astronomical unit (AU), the distance between the Sun and Earth (~1.5 10^8 km), typical solar wind densities and speeds are approximately 5 cm^{-3} and 400 km/s, respectively. Under disturbed conditions they can rise to greater than 20 cm^{-3} and 1,000 km/s, respectively. The dynamic pressure of the solar wind (~1 nano-Pascal (nPa)) compresses the Earth's magnetic field on the dayside and extends it into a long cylinder called the magnetotail. The convenient unit for measuring distance in the magnetosphere is an Earth radius (1 R_E = 6387 km). Under typical conditions the subsolar magnetopause is at ~10 R_E . When conditions become disturbed the solar wind's dynamic pressure can exceed 10 nPa and the magnetopause is pushed earthward of geostationary orbit (~6.6 R_E).

Table 1. Solar Wind Characteristics		
Parameter	Typical	Disturbed
Density	5 - 10 cm^{-3}	20 - 100 cm^{-3}
Velocity	400 km/s	700 km/s
Pressure	1 - 2 nPa	> 10 nPa
IMF	5 - 10 nT	20 - 60 nT

4

BO-000027 addition -
SFOML-WING-6-14.pdf

CTF091-1760

A weak interplanetary magnetic field (IMF) is carried by the solar wind and exerts great influence on geospace weather. Typical values of the IMF are in the 5 to 10 nanotesla (nT) range; this can grow to > 40 nT during disturbed times. The IMF interacts efficiently with the Earth's magnetic field through a process called magnetic merging when the IMF has a southward component. In the vicinity of the Earth there are three distinct magnetic topologies: interplanetary field lines with both "feet" in the solar wind, closed magnetic field lines with both "feet" on Earth, and open field lines with one "foot" in the solar wind and the other on the Earth. The region of open field lines is called the polar cap. Energetic particles in the solar wind have fairly easy access to the ionosphere at polar cap latitudes. The solar wind and IMF impose a potential across the polar cap that ranges from a few tens of kilovolts (kV) during magnetic quiet times to > 200 kV during large magnetic storms. Associated electric fields drive currents in the magnetosphere and ionosphere that produce observable magnetic perturbations on the ground. The three most common measures of geomagnetic activity are the three-hour Kp index of solar particle effects, the one-minute averaged auroral electrojet (AE) index, and the one-hour averaged Disturbance Storm Time (Dst) index (Table 2). Kp reflects the intensity of magnetic disturbances measured at mid latitude stations; it varies from < 3 during quiet / moderate times to > 5 under disturbed conditions. AE is a measure of currents flowing in the ionosphere at auroral latitudes; it has values of < 100 nT during quiet times and > 300 nT during disturbances. The Dst index is a globally averaged measure of the stormtime ring current's intensity. During large magnetic storms the westward ring current produces perturbations < -200 nT at low-latitude magnetic stations. On February 1, 2003 around the time of Columbia's reentry shortly before 1400 GMT, geomagnetic indices were low; Kp ranged from 1- to 3+ and Dst measured between +30 and +34.

Table 2. Geomagnetic Indices		
Characteristic	Typical	Disturbed
Kp: 3 - hr midlatitude index	< 3	> 5
Dst: 1 - hr ring current	> -50 nT	< -100 nT
AE: 1 - min auroral electrojet	< 100 nT	> 300 nT

2.3 Solar Effects

Figure 1 shows a hydrogen alpha image of the Sun taken on February 1, 2003 at Learmonth, Australia, from the National Oceanic and Atmospheric Administration (NOAA) Space Environment Center's Solar Image Archive. It indicates that the chromosphere was relatively quiescent. Also noted are the time scales and geospace locations of three types of solar activity that impact space weather, coronal mass ejections, energetic particles, and flares. For future reference we note that CMEs have broad effects throughout geospace. However, the most significant effects of solar energetic particles (SEPs) are confined to magnetic latitudes of the polar cap.

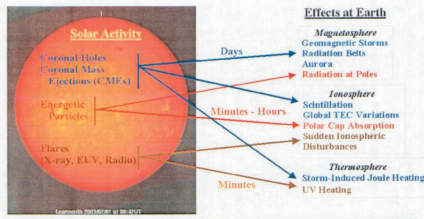
Figure 2 illustrates the significant differences between simultaneous views of a quiet photosphere in visible light and a turbulent corona seen at extreme ultra violet (EUV) wavelengths. Figure 3 shows the early stage development of a CME as observed

5

BO-000027 addition -
SFOML-WING-6-14.pdf

CTF091-1761

by a white light coronagraph on the Solar and Heliospheric Satellite (SOHO) which orbits the first Lagrangian point, about one million miles in front of the Earth. Figure 4a plots the range of SEP spectra observed in the solar wind, and Figure 4b demonstrates SEP effects on the active sensor array on SOHO. Random light speckles are excited as MeV SEPs running ahead of a CME pass through elements of the charge coupled device array of the SOHO coronagraph. Fortunately, this type of upset is temporary. A visible-light imager on the Polar satellite acquired the picture of the auroral oval in Figure 4c. It shows that during the great magnetic storm of Bastille Day, July 14, 2000, auroral optical emissions, caused by the impact of energetic electrons on the upper atmosphere, were detected in the southern part of the United States.



The Sun is the principal source of disturbances in the geospace environment

Figure 1. Hydrogen alpha image of the Sun taken on February 1, 2003 at Learmonth, Australia, along with time scales and geospace locations of three types of solar activity that affect space weather.

6

BO-000027 addition -
SFOML-WING-6-14.pdf

CTF091-1762

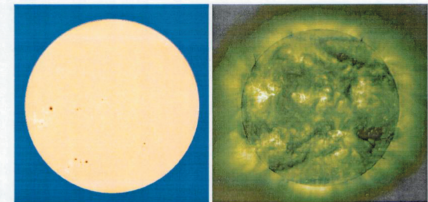


Figure 2. Simultaneous views of a quiet photosphere in visible light and a turbulent corona seen at EUV wavelengths.

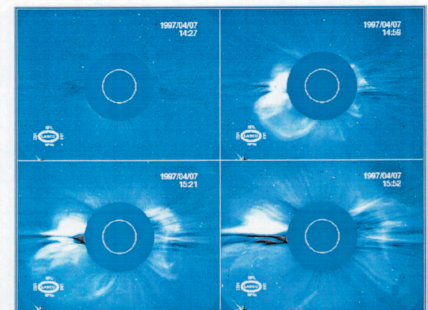


Figure 3. Early stage development of a CME as observed by a white light coronagraph on the SOHO satellite.

7

BO-000027 addition -
SFOML-WING-6-14.pdf

CTF091-1763

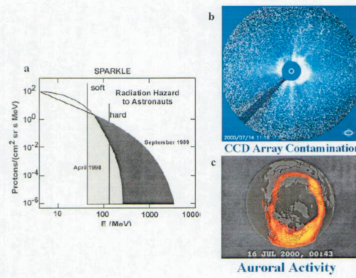


Figure 4. Plot (a) shows the range of SEP spectra observed in the solar wind, (b) SEP effects on the active sensor array on SOHO, and (c) a visible-light image of the auroral oval from the Polar satellite.

Figure 5 shows the most extreme compressional effect of a CME ever observed in the magnetosphere detected by the Combined Release and Radiation Effects Satellite (CRRES) at the onset of the great magnetic storm of March 24, 1991. CRRES flew in a geostationary transfer orbit with perigee at an altitude of ~390 km and apogee at ~6.6 R_E . Figure 5 is a plot of the distribution of protons with energies of ~10.7 MeV in distance from the Earth as a function of orbit number. Attention is directed to the sudden increase in the flux of protons during orbit #587 at radial distances between 2 and 2.5 R_E from the center of the Earth.

CRRES measurements show that the injected high-energy particles were trapped in the magnetosphere and did not have access to the ionosphere. A sudden increase in flux was observed during the inbound pass at ~03:45 UT. This was the first sign of shock-accelerated protons. CRRES then passed through the inner radiation belt, behind the Earth and crossed the spatially extended new radiation belt. The initial injection was narrowly confined in energy to near 40 MeV. During the outbound pass the energies of newly trapped protons filled the 10 to 70 MeV range. These protons were observed continuously for the next seven months (Figure 5) until the spacecraft's battery failed.

8

B0-000027 addition -
SFOML-WING-6-14.pdf

CTF091-1764

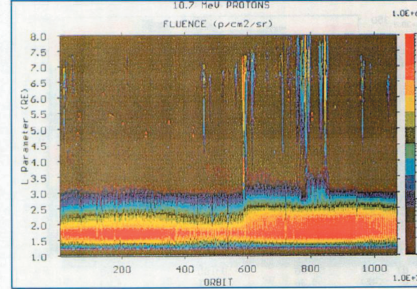


Figure 5. CRRES data from March 24, 1991 show the formation of a new radiation belt.

Modeling studies suggest that the protons first observed near 2 R_E were initially trapped in the outer magnetosphere. They were then accelerated by an intense, earthward-propagating compressional magnetohydrodynamic wave excited after a CME shock impacted the magnetopause. The wave also accelerated and transported energetic electrons into the inner radiation belt. We must emphasize that this was a singular event. The measured amplitude of the compressional magnetic wave that reached the ground at Boulder, Colorado, was 184 nT. During most storms the ground perturbation due to the sudden compression of the magnetosphere is a few tens of nanoTesla.

2.4 Radiation Effects

The CRRES mission objective was to determine the survivability of microelectronic components in natural space-radiation environments. Current national policy calls for using commercial, off the shelf components whenever possible. Without detailed specifications of the radiation environments in which the microelectronic components must operate, this policy would significantly increase the vulnerability of national space assets. The national laboratories are working to reduce this vulnerability in a number of ways, including the Air Force Research Laboratory's (AFRL's) Compact Environmental Anomalies Sensor Experiment (CEASE). CEASE provides real time measurements of total radiation dose to warn of potential space hazards and facilitate

9

B0-000027 addition -
SFOML-WING-6-14.pdf

CTF091-1765

analysis of anomalies such as single event upsets and deep dielectric charging. Other methods include improved prediction and monitoring of space environment hazards and developing practical ways to accelerate the loss of trapped particles from the radiation belts. Figure 6 summarizes the main radiation hazards to which space systems are exposed. The first, called a single event upset, occurs when MeV protons pass through the shielding of microelectronic components leaving trails of ionization and currents that can trigger false commands or altered memory states. Long exposure to doses of energetic protons degrades and destroys the functionality of microelectronic devices.

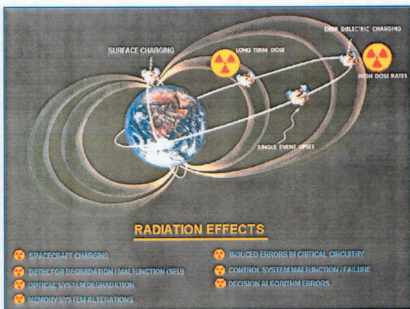


Figure 6. Primary radiation hazards to space systems.

Unexpectedly, the most common upset observed in the CRRES mission derived from a process called deep dielectric charging. This phenomenon occurs when the insulation wrapped around a wire is exposed to prolonged doses of electrons with energies > 100 keV. These energetic electrons penetrate far enough into dielectrics that secondary electrons cannot escape. If enough space charge builds up within the dielectric, Coulomb repulsive forces can exceed the cohesive strength of the material. Charge suddenly starts moving toward the wire and appears as a current burst. The time history of CRRES suggests that dielectrics pass through a long period of slow degradation before deep dielectric events become common. Because the Columbia accident involved failures of insulating tiles, we give special consideration to the susceptibility of the shuttle to deep dielectric charging below.

10

B0-000027 addition -
SFOML-WING-6-14.pdf

CTF091-1766

2.5 Equatorial Plasma Bubbles

The final two figures of the tutorial (Figures 7 and 8) consider a phenomenon known as equatorial plasma bubbles that disrupt transionospheric radio communications. In the post sunset ionosphere, plasma below ~300 km quickly recombines leaving the F layer supported only by the Earth's magnetic field. This is fertile ground for the development of a classic Rayleigh-Taylor instability where a light fluid supports a heavy fluid. Plasma on long magnetic flux tubes interchanges with low-density bubbles that percolate upwards at speeds up to a few kilometers per second. AFRL's Scintillation Network Decision Aid (SCINDA) network (Figure 7) is a ground-based sensor network designed to detect ionospheric scintillations. SCINDA receivers use spaced antenna measurements to provide an estimate of the drift of ionospheric irregularities. The turbulent bubbles and their interactions with radio waves have been modeled extensively in computer simulations at the Naval Research Laboratory. They have also been observed by visible and ultraviolet sensors as elongated streaks of diminished airglow at wavelengths of 6300 and 1356 Å as shown in Figure 8 from the Global Ultraviolet Imager (GUVI) instrument on the Thermosphere, Ionosphere, Mesosphere Energetics and Dynamics Mission (TIMED) satellite. Equatorial plasma bubbles are an evening sector phenomenon and cannot have been responsible for intermittent communications disruptions experienced during Columbia's reentry.

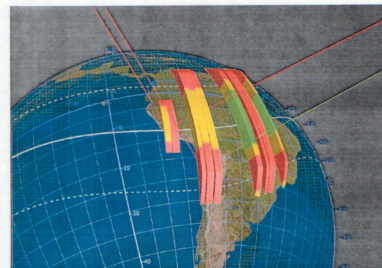


Figure 7. AFRL's SCINDA network of ground-based sensors is designed to detect ionospheric scintillations. SCINDA receivers use spaced antenna measurements to provide an estimate of the drift of ionospheric irregularities.

11

B0-000027 addition -
SFOML-WING-6-14.pdf

CTF091-1767



Figure 8. Equatorial plasma bubbles observed by the GUVI visible and ultraviolet sensors on the TIMED satellite.

3.0 Space Weather Conditions on February 1, 2003

The final breakup of Columbia occurred shortly after 1400 UT on February 1, 2003. To understand prevailing space weather conditions and their possible effects on the Columbia accident we have examined measurements from many satellite and ground observatories during the reentry period.

There are several different ways to present geophysical measurements made on the day of the Columbia accident. Interplanetary observations from the Advanced Composition Explorer (ACE) satellite set the stage for all that follows. Somewhat arbitrarily we have chosen to group the remaining measurements from (1) polar-orbiting satellites of the Defense Meteorological Satellite Program (DMSP) and the NOAA Polar Operational Environmental Satellite (POES) program in low Earth orbit (LEO), (2) Los Alamos National Laboratory (LANL) and NOAA Geostationary Operational Environmental Satellites (GOES) in geostationary orbit, and (3) ground observatories.

3.1 Interplanetary Measurements from ACE

The first satellite to observe interplanetary disturbances approaching Earth is the ACE that flies in a halo orbit around the first Lagrangian point about one million miles upstream of the Earth in the solar wind. Typically it takes the better part of an hour for

12

B0-000027 addition -
SFOML-WING-6-14.pdf

CTF091-1768

the solar wind/IMF observed by ACE to reach the Earth. The traces in Figure 9a show fluxes of energetic protons passing ACE plotted as a function of UT on February 1. The middle three plots indicate that conditions were steady until ~18:00 UT when the fluxes of protons with energies between 0.1 and 2 MeV rose sharply. The increased flux occurred ~4 hours after the accident and therefore had no impact upon it. Figure 9b shows the solar wind density (top plot), the IMF magnitude (second plot), and Z (north south), Y (east-west) and X (Sun-Earth) components of the IMF (middle to bottom plots). The solar-wind density was steady and unusually low ($< 1 \text{ cm}^{-3}$) throughout the period of interest. At ~13:00 UT the IMF magnitude increased from 9 to 12 nT and the solar wind speed rose from ~400 to 500 km/s (not shown). The middle plot indicates that until 17:30 UT the Z component of the IMF was northward. The observed interplanetary changes should not have interacted strongly with the Earth's magnetic field. This conjecture is borne out by satellite and ground measurements presented below.

At 1344 UT on February 1, 2003 the staff on duty at Space Weather Operations in Boulder, Colorado, issued a warning for a Sudden Impulse, a characteristic step-wise jump in the horizontal geomagnetic field component on the dayside. This warning was based on observations of the solar wind speed increase of ~25%, seen by a plasma sensor on ACE at 1308 UT. This increase in speed was accompanied by a small increase in the magnetic field, but no corresponding increase in solar wind density (Figure 9). Typical shocks show simultaneous jumps in speed, density, and magnetic field. As time passed and no subsequent shock or impulse was observed in data acquired nearer to the Earth, this warning came to be regarded as a false alarm.

3.2 LEO Measurements from DMSP

Figures 10 - 12 present measurements from three DMSP satellites F13, F14, and F15. DMSP satellites fly in circular polar orbits at an altitude of ~840 km. At an inclination of 98.0° their orbital planes remain at fixed local time (LT) with respect to the sun. The orbit of DMSP F13 is near the dawn-dusk terminator. The orbital planes of DMSP F14 and F15 are near the 09:00 - 2100 LT meridian.

Data from the three DMSP satellites are plotted as functions of UT, magnetic latitude, and magnetic local time (Figures 10-12). The top two plots of each figure show the fluxes of electrons and ions with energies between 30 eV and 30 keV in an energy-versus-time color spectrogram format. The third plot gives the density of ionospheric plasma at the spacecraft altitude. The vertical (green) and horizontal (purple) components of ion drift across the satellite trajectory are presented in the fourth plot. The horizontal drift component is directly proportional to the electric field component along the spacecraft trajectory. Integration of this electric field component along the trajectory gives the cross polar cap potential. The bottom plot gives the three components of magnetic perturbations due to field-aligned currents that electrically couple the magnetosphere and ionosphere. The component of the Earth's magnetic field shown in green is highly correlated with horizontal drift measurements. Drift meters and magnetometers on DMSP satellites serve as voltmeters and ammeters to monitor characteristics of the global magnetosphere-ionosphere circuit.

13

B0-000027 addition -
SFOML-WING-6-14.pdf

CTF091-1769

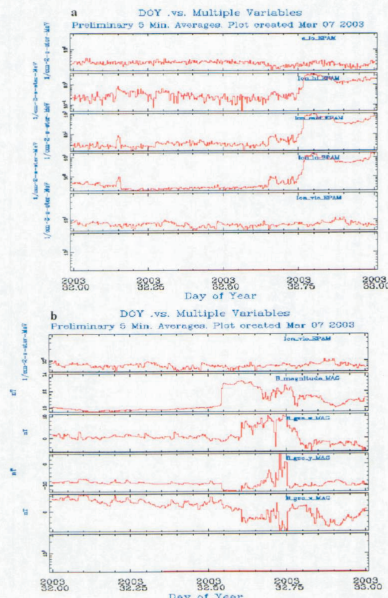


Figure 9. Measurements from ACE on February 1, 2003.

14

B0-000027 addition -
SFOML-WING-6-14.pdf

CTF091-1770

The gap in DMSP F14 measurements between 13:42 and 13:46 UT occurred in the evening sector of the polar cap and probably reflects an outage that occurred while data were being transmitted to ground. Electron and ion data from all DMSP spacecraft indicate moderate to low auroral activity during the time of Columbia's reentry. This is especially true in the dawn LT sector. Drift meter and magnetometer measurements are also consistent with weak to moderate magnetosphere-ionosphere coupling. In particular we note that neither plasma velocities nor magnetic perturbations due to field-aligned (Birkeland) currents measured by the three DMSP satellites showed any sign of an electromagnetic pulse indicating that the magnetosphere underwent a sudden compression near the time of Columbia's reentry. Data from ground magnetometers also show no sign of a magnetic compression event.

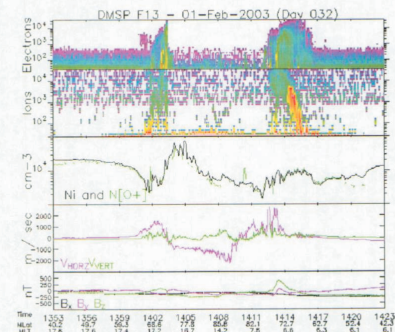


Figure 10. DMSP F13 measurements for February 1, 2003, plotted as functions of UT, magnetic latitude, and magnetic local time. The top two plots show fluxes of electrons and ions from 30 eV to 30 keV in an energy-versus-time color spectrogram. The third plot gives the density of ionospheric plasma at spacecraft altitude. Vertical (green) and horizontal (purple) components of ion drift across the satellite trajectory are presented in the fourth plot. The bottom plot gives the three components of magnetic perturbations due to field-aligned currents that electrically couple the magnetosphere and ionosphere.

15

B0-000027 addition -
SFOML-WING-6-14.pdf

CTF091-1771

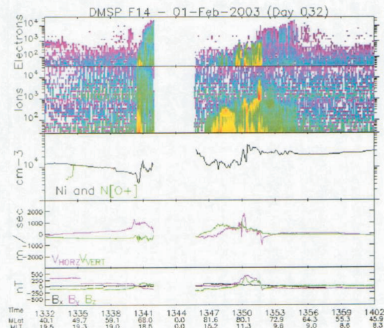


Figure 11. DMSP F14 measurements for February 1, 2003 in the same format as shown in Figure 10.

16

BO-000027 addition -
SFOML-WING-6-14.pdf

CTF091-1772

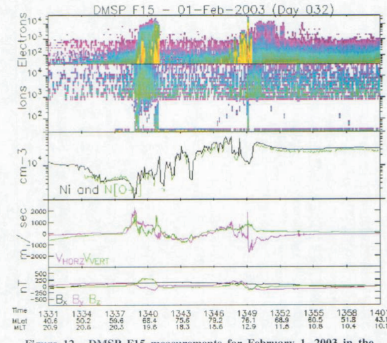


Figure 12. DMSP F15 measurements for February 1, 2003 in the same format as shown in Figure 10.

17

BO-000027 addition -
SFOML-WING-6-14.pdf

CTF091-1773

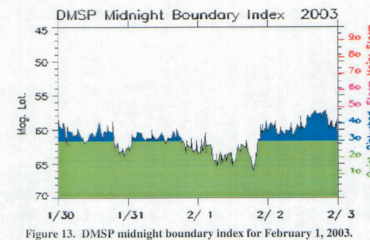


Figure 13. DMSP midnight boundary index for February 1, 2003.

Figure 13 takes the auroral electron boundaries observed by the DMSP satellites and projects them to the midnight meridian. The Air Force Weather Agency (AFWA) uses the latitude of auroral boundaries at midnight as an operational tool to specify current values of the Kp index. Boundary locations between 12:00 and 14:00 UT indicate magnetically quiet conditions. Kp entered the disturbed range late on February 1, 2003. Both then and on the following day geomagnetic conditions never approached the major storm status of either March 24, 1991, when CRRES observed the birth of a new radiation belt, or Bastille Day July 14, 2000, when auroral emissions appeared in the skies over the southern part of the United States.

3.3 LEO Measurements from POES

NOAA POES 15, 16, and 17 satellites also fly in sun-synchronous circular polar orbits, but near the 02:00 - 14:00 LT meridian. These satellites carry particle detectors covering the energy range from a few hundred eV to ~1 MeV. Standard estimates of the total energy input to the high-latitude ionosphere due to precipitating particle fluxes, as measured by the NOAA satellites, were in the low to moderate range near the time of Columbia's reentry. Although POES measurements were made at local times different from those of DMSP, their observations were similar, showing no indication of a geomagnetic disturbance during the period of interest.

Figures 14 and 15 show the trajectories of the NOAA POES 16 satellite for the full day of February 1, 2003. The trajectories are marked in color to indicate the relative fluxes of protons with energies between 250 and 800 keV and of electrons with energies > 300 keV. The color scales compare fluxes measured on February 1 with the median values observed at that location during the entire previous year. The data show "no higher than normal" (yellow) occurrences of energetic fluxes in the region over and to the east of Chile and Argentina, called the South Atlantic Anomaly (SAA). Within the SAA the Earth's magnetic field is weaker than average and allows radiation belt protons and electrons to penetrate more deeply than normal into the upper atmosphere. The 39° inclination of the STS-107 orbit placed Columbia within the SAA for a small portion of the mission. This was the only place during the entire mission where Columbia was exposed to energetic particles.

18

BO-000027 addition -
SFOML-WING-6-14.pdf

CTF091-1774

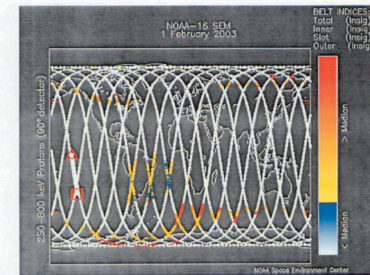


Figure 14. Relative fluxes of protons with energies between 250 and 800 keV from the NOAA POES 16 satellite.

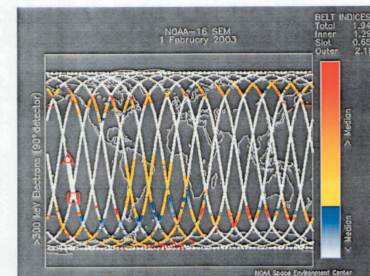


Figure 15. Relative fluxes of electrons with energies > 300 keV from the NOAA POES 16 satellite.

19

BO-000027 addition -
SFOML-WING-6-14.pdf

CTF091-1775

3.4 Charging Effects

The Columbia accident involved a serious breach of one or more heat tiles on the leading edge of the orbiter's left wing. We must then ask if there is any known space weather effect that could possibly have caused such a breach. In principle, the answer appears to be "yes." If the tiles were subject to prolonged exposure to intense fluxes of electrons with energies >100 keV, space charge could build up within the non-conducting materials. Electrons with lower energies would be stopped in the surface layer of the tiles and would cause surface charging. Electrons with energies >> 1 MeV would simply pass through the tiles. In neither the low nor extremely high energy cases would damage occur. During the Tethered Satellite System mission in 1996, Columbia charged to around a kilovolt with respect to the local plasma but suffered no ill effects.

As indicated in our discussion of deep dielectric charging (Figure 6), if sufficient space charge builds up within an insulating material, Coulomb repulsion forces eventually overwhelm material bonds. If breakdown occurs, a surge of plasma migrates quickly either to the nearest metal or to the outer surface. In the first case, the discharge current would flow to the shuttle's metal frame, to which all other circuits are grounded. Sudden changes in the ground potential induce current surges in all orbiter circuits simultaneously that would be identifiable in the mission telemetry stream. In the second case, negative space charge trapped within the dielectric would attract positive ions from the ionospheric plasma to the outer surfaces of the non-conducting tiles. A massive discharge to the outer surface could cause a breach in a critical surface that would widen as frictional interactions with the atmosphere increased during reentry. Such an event would not easily be identifiable in the telemetry data stream.

Is it likely that Columbia was exposed to a significant level of deep dielectric charging during the course of the mission or that a breach formed in a tile surface? The answer to both questions is negative. The orbital inclination of ~ 39° generally kept Columbia far from significant exposure to radiation in the "horns of the radiation belts" and auroral oval and from SEPs in the polar cap. The only exception lasted a few minutes each day as its orbital trajectory carried Columbia through part of the SAA. The SAA centers near 50° S, 60° W. To specify Columbia's exposure we have examined fluxes of electrons with energies >100 keV observed by the NOAA POES 15, 16, and 17 satellites in two orthogonal look directions while crossing the SAA (Figure 15) between January 16 and February 1, 2003. As a worst case scenario, we assumed that Columbia spent 600 seconds each day within the SAA and that every > 100 keV electron that struck a tile became embedded within it and no charge escaped. The estimated dose was -1.22×10^3 Coulombs/m². Assuming a dielectric coefficient of 5, Gauss's law predicts a maximum electric field of $\sim 10^3$ V/m. This is a factor of 3 below breakdown electric fields for air and roughly an order of magnitude below breakdown for most insulating solids. Finally, a cursory glance at Figure 15 indicates that in a 39° inclination orbit, Columbia was more exposed to SAA radiation than orbiters in the standard 28.5° inclined orbit. However, Columbia was much less exposed than orbiters on extended missions to service the International Space Station.

20

BO-000027 addition -
SFOML-WING-6-14.pdf

CTF091-1776

Silica fibers constitute more than 99% of the shuttle tiles. Individual fibers are <3.2 mm long, between 1.2 and 4 microns in diameter, and are sintered together. The net density is 0.145 g/cc and the dielectric constant is 1.13. A borosilicate glass cover between 0.23 and 0.38 mm thick surrounds the tile fibers. In anticipation of polar-orbiting shuttle missions, sample tiles were irradiated by energetic electrons beams at AFRL to levels of $\sim 10^3$ Coulombs/m². This is similar to the estimated dose applied to Columbia in the SAA. In the experiments the tiles were observed to hold charges for days in the vacuum chamber. Non-destructive, prebreakdown pulses were observed whenever the induced electric field exceeded 10^3 V/m. Full breakdown of tile material never occurred. A full description of the experiments and their results appears in "Charging/discharging of space shuttle tile material under irradiation", by A. R. Frederickson and A. L. Chesley, *IEEE Trans. Nucl. Sci.*, 30, 4296-4301, 1983.

3.5 Geostationary Orbit Measurements

We next turn our attention to observations of energetic particles measured by sensors on five LANL and two GOES satellites that orbit the Earth at geostationary altitude. The left side of Figure 16 shows fluxes of protons with energies between 50 and 400 keV. Electron fluxes measured in the 50 to 315 keV range are shown in the right plot. The yellow and blue vertical lines crossing each spectrogram indicate when a particular satellite crossed the midnight and noon meridians, respectively. Except for small flux increases observed in the lowest (50 keV) channels near 14:00 UT, the environments sampled by all LANL satellites were very steady in the hours leading up to Columbia's reentry. Similarities between proton and electron spectra detected by widely spaced LANL satellites indicate that the geostationary environment was uniform. Consistent with ACE, LEO, and ground measurements, most of the geomagnetic activity encountered by the LANL satellites occurred after 20:00 UT.

21

BO-000027 addition -
SFOML-WING-6-14.pdf

CTF091-1777

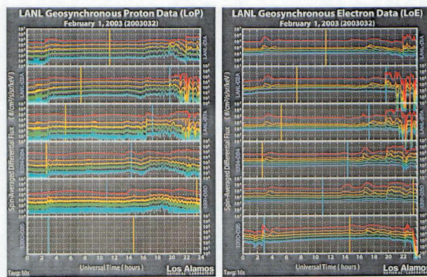


Figure 16. Fluxes of protons with energies between 50 and 400 keV (left) and electron fluxes measured in the 50 to 315 keV range (right) from LANL satellites.

A variety of space environmental parameters measured by GOES satellites appear in the next four figures. Figure 17 depicts the flux of electrons > 600 keV and > 2 MeV, as measured by two GOES satellites for the days January 31 through February 2, 2003. The only noteworthy characteristic is that the fluxes were somewhat elevated for the three-day period. Figure 18 shows fluxes of protons with energies > 10, 50, and 100 MeV for the same three days as measured by GOES 8 located near 75° W. The energetic proton fluxes show no enhancements in magnitude and attest to the presence of persistently benign conditions at geostationary orbit.

Solar flares are monitored by their X-ray outputs. Both the GOES 8 and 10 satellites carry sensors to measure X-ray fluxes in the 0.05 - 0.4 nm and 0.1 - 0.8 nm wavelength bands. Between January 31 and February 2, 2003 (Figure 19), occasional solar X-ray flares occurred. Two X-ray spikes were observed on February 1. However, there is no known association between the occurrence of X-ray photons near Earth and plasma disturbances that would have a significant impact on the predawn ionosphere at reentry altitudes of Columbia.

22

BO-000027 addition -
SFOML-WING-6-14.pdf

CTF091-1778

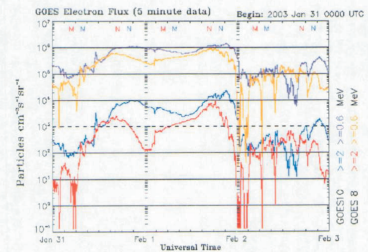


Figure 17. Flux of electrons > 600 keV and > 2 MeV as measured by two GOES satellites for January 31 through February 2, 2003.

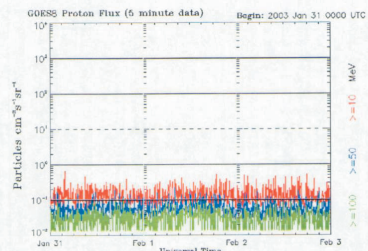


Figure 18. Fluxes of protons with energies greater than 10, 50, and 100 MeV for January 31 through February 2, 2003, as measured by GOES 8 located near 75° W.

23

BO-000027 addition -
SFOML-WING-6-14.pdf

CTF091-1779

Figure 20 is a composite of four data sets that from top to bottom show: GOES proton fluxes (Figure 18), GOES electron fluxes (Figure 17), the Hp (nearly north-south) component of the Earth's field measured by GOES, and the Kp ground index described previously. This stack plot is useful for comparing various data acquired at the same time. Focusing on the first 15 hours of February 1, we see that regular and quiet conditions are indicated in all four measurements.

It is useful to return to the global distribution of energetic (> 300 keV) electron fluxes observed by NOAA POES 16 as shown in Figure 15 which illustrates the relative fluxes of these particles. The fact that above-average fluxes were detected at high latitudes during virtually all passes is consistent with the presence of relatively high fluxes of > 2 MeV electrons observed by GOES at geostationary orbit (Figure 17). The footprint of the SAA is clearly seen. Elevated electron fluxes were mostly confined to latitudes higher than those accessible to Columbia's low inclination.

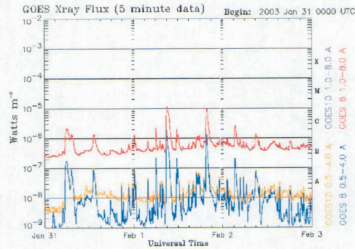


Figure 19. Measurements of X-ray fluxes in the 0.05 - 0.4 nm and 0.1 - 0.8 nm wavelength bands from GOES 8 and 10 satellites for January 31 through February 2, 2003.

24

B0-000027 addition -
SFOML-WING-6-14.pdf

CTF091-1780

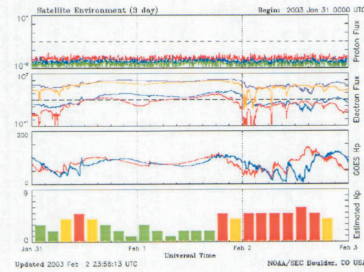


Figure 20. Composite of four data sets that from top to bottom show: GOES proton fluxes, GOES electron fluxes, the Hp (nearly north-south) component of the Earth's field measured by GOES, and the Kp ground index described previously for January 31 - 2 February 2003.

3.6 Ground Based Measurements

Our satellite-based estimate of low geomagnetic activity is confirmed by values of the AE and Dst indices measured on February 1, 2003 (Figure 21). During the time of Columbia's reentry, AE and Dst had values of ~100 nT and +34 nT, respectively. Significant auroral electrojet activity only began near 20:00 UT, about six hours after the accident. Steady positive values of Dst indicate that the ring current was inactive. The ring current is mostly carried by ions with energies > 10 keV that drift to the westward in the magnetosphere and produce negative perturbations to the Earth's magnetic field.

Magnetometers distributed over the surface of the Earth monitor the behavior of the Earth's magnetic field. These measurements reflect effects of electrical currents flowing in the ionosphere at altitudes near 120 km. Figures 22 and 23 are records of magnetic field measurements from Kiruna, Sweden, and Gakona, Alaska, respectively. Both of these instruments detected normally quiet conditions until late on February 1, when the effects of a CME began to drive relatively intense ionospheric currents. We also examined the record acquired at the Huancayo, Peru, station at the magnetic equator (not shown). If a CME-driven shock impacted the dayside magnetopause near 14:00 UT, a sudden increase in the north-south component of the magnetic field would have been

25

B0-000027 addition -
SFOML-WING-6-14.pdf

CTF091-1781

detected at Huancayo. Instead, measurements on February 1, 2003 only show the diurnal magnetic variations characteristic of the solar-quiet current system in the ionosphere.

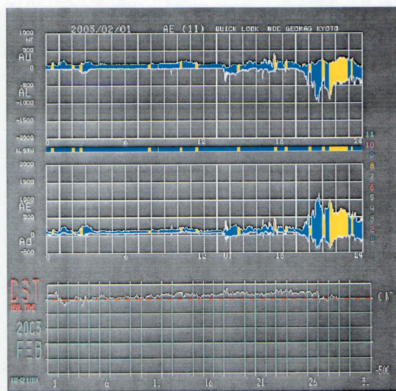


Figure 21. AE and Dst measurements for February 1, 2003.

Finally, to determine whether intense fluxes of SEPs had somehow passed undetected through geostationary and low Earth orbits, we examined fluxes measured at ground-based neutron monitors in Moscow and Apatity, Russia, Oulu, Finland, and Lomnický štít, Slovakia. These stations were in the afternoon LT sectors while Columbia was reentering the Earth's atmosphere. On February 1, 2003 these monitors detected only diurnal variations that appear to be similar in form and intensity to those recorded on other days of the month. We conclude that unusually large SEP fluxes did not impact the upper atmosphere near the time of the Columbia's reentry.

26

B0-000027 addition -
SFOML-WING-6-14.pdf

CTF091-1782

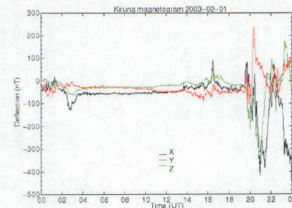


Figure 22. Magnetic field measurements from Kiruna, Sweden for February 1, 2003.

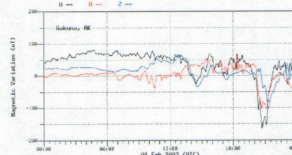


Figure 23. Magnetic field measurements from Gakona, Alaska for February 1, 2003.

4.0 Summary and Conclusions

We have examined a wide variety of space related parameters measured by satellite and ground based sensors on February 1, 2003. All indications point to the fact that Columbia's reentry occurred during a period of low geomagnetic activity. It is difficult to imagine a more benign space weather environment for Columbia to start its reentry. Signs of moderate activity were not observed until late in the day, six or more hours after the accident. Were it not for the fact that the accident happened on February 1, 2003, it is unlikely that space-weather investigators would have given the day more than cursory inspection.

27

B0-000027 addition -
SFOML-WING-6-14.pdf

CTF091-1783

5.0 Acronyms

Å	Angstrom
ACE	Advanced Composition Explorer
AE	Auroral electrojet
AFRL	Air Force Research Laboratory
AFWA	Air Force Weather Agency
AU	Astronomical Unit
CAIB	Columbia Accident Investigation Board
CEASE	Compact Environmental Anomalies Sensor Experiment
cm	centimeter
CME	Coronal Mass Ejection
CRRES	Combined Release and Radiation Effects Satellite
DMSP	Defense Meteorological Satellite Program
Dst	Disturbance Storm Time
EUV	Extreme ultraviolet
eV	electron volt
GMT	Greenwich Mean Time
GOES	Geostationary Operational Environmental Satellite
GUVI	Global Ultraviolet Imager
IMF	Interplanetary Magnetic Field
km	kilometer
Kp	index of solar particle effects on the Earth's magnetic field
keV	thousand electron volts
kV	kilovolt
LANL	Los Alamos National Laboratory
LEO	low Earth orbit
LT	local time
MeV	million electron volts
NOAA	National Oceanic and Atmospheric Administration
nPa	nano-Pascal
nT	nano-Tesla
POES	Polar Operational Environmental Satellite
R _e	Earth radius
SAA	South Atlantic Anomaly
SCINDA	Scintillation Network Decision Aid
SEP	Solar energetic particles
SOHO	Solar and Heliospheric Observatory
TIMED	Thermosphere, Ionosphere, Mesosphere Energetics and Dynamics satellite
UT	Universal Time (equivalent to GMT)

28

B0-000027 addition -
SFOML-WING-6-14.pdf

CTF091-1784

THIS PAGE INTENTIONALLY LEFT BLANK